Soft Matter

PAPER

View Article Online
View Journal | View Issue

Cite this: *Soft Matter*, 2014, **10**, 9110

An experimental and simulation study on the self-assembly of colloidal cubes in external electric fields

Hanumantha Rao Vutukuri,* Frank Smallenburg, Stéphane Badaire, Arnout Imhof, Marjolein Dijkstra and Alfons van Blaaderen*

Received 10th August 2014
Accepted 11th September 2014

DOI: 10.1039/c4sm01778a

www.rsc.org/softmatter

When a suspension of colloidal particles is placed in an oscillating electric field, the contrast in dielectric constant between the particles and the solvent induces a dipole moment in each of the colloidal particles. The resulting dipole–dipole interactions can strongly influence the phase behavior of the system. We investigate the phase behavior of cube-shaped colloidal particles in electric fields, using both experiments and Monte Carlo simulations. In addition to a string fluid phase and a body centered tetragonal (BCT) crystal phase, we observe a columnar phase consisting of hexagonally ordered strings of rotationally disordered cubes. By simulating the system for a range of pressures and electric field strengths, we map out the phase diagram, and compare the results to the experimentally observed phases. Additionally, we estimate the accuracy of a point-dipole approximation on the alignment of cubes in string-like clusters.

Introduction

The main goal of the field of colloidal self-assembly is the creation of new functional materials *via* the spontaneous self-organization of colloids: building blocks on the nano- to micrometer scale.[1–5] The structure of these materials is mainly determined by the interactions between the individual colloidal particles, their shape, and their concentration. Thus, in order to control the self-assembled structures, one typically has to change the inherent properties of the particles, by *e.g.* synthesizing new colloids with different shapes, sizes, or surface chemistries. Alternatively, the interactions of colloidal particles can be changed by modifying their environment. For example, depletion attractions can be induced by adding non-adsorbing polymers to a colloidal suspension, and the range of interactions between charged colloids can be tuned by changing the ion concentration in the solvent. Additionally, external electric or magnetic fields can be used to induce dipolar interactions between the particles. Even for simple spherical particles, oscillating external electric fields have proven to be a versatile tool for directing the self-assembly of colloidal particles into strings,[6–9] sheets[10–12] or crystal structures.[13–15]

When an oscillating electric field is applied to a colloidal suspension, the difference in dielectric constant between the colloids and the solvent induces a polarization which can often for a certain range of distances be approximated by a dipole moment centered in each colloid, and parallel to the external field. The resulting dipole–dipole interactions between different particles favor the alignment of the particles along the field direction, drastically impacting the phase behavior of the colloidal dispersion.[13–15] For monodisperse spherical particles in a uniaxial external field, it has been shown by computer simulations that the bulk phase behavior exhibits a body-centered tetragonal (BCT) and a hexagonally close-packed (HCP) crystal phase as well as the face-centered cubic (FCC) crystal typical for hard-sphere systems.[16,17] Experimentally, only the BCT and FCC phases have been observed.[18] The variety of self-assembled structures can be further enhanced by applying fields to binary systems of spheres,[19,20] or by making use of biaxial or even triaxial fields.[10–12,21,22] The same method can be used to induce dipolar interactions in colloidal particles of any shape, such as rods[23,24] or dumbbells.[25] In addition to changing interparticle interactions, external fields also tend to align anisotropic particles: dipolar interactions within each particle typically favor the alignment of the longer axis of the particle along the direction of the field.[26] This technique is commonly used in liquid-crystal displays to change the director of a nematic phase in order to alter its optical properties. Both the orientation-dependent energy and the dipolar interactions have been calculated for a wide range of odd-shaped particles such as dumbbells, bowls, cubes, rods, and platelets, using the coupled dipole method.[27–29] In this work, we explore the effect of an external uniaxial field on the phase behavior of cube-shaped colloidal particles, using both experiments and simulations.

Methods to synthesize cubes on the micrometer[30,31] and the nanometer scale[32–36] have recently generated renewed interest

Soft Condensed Matter, Debye Institute for NanoMaterials Science, Utrecht University, 3584 CC Utrecht, The Netherlands. E-mail: H.R.Vutukuri@uu.nl; A.vanBlaaderen@uu.nl

also in the phase behavior of cube-shaped particles.[31,37,38] Several simulation studies have investigated the phase behavior of cubic and similar particles, resulting in phase diagrams for hard cubes,[39,40] truncated cubes,[41] tetragonal parallelepipeds[42] and colloidal superballs,[43,44] as well as for a range of polyhedral shapes with varying degrees of anisotropy.[40] A simulation study on cubes with a permanent dipole moment, as might be expected for certain semiconductor nanoparticles, has shown that these can self-assemble into wires, sheets or ring-like structures depending on the orientations of the dipoles with respect to the cubes.[45] Here, we study micron-sized cubes of single crystalline neighborite ($NaMgF_3$) in a MHz electric field which is fast enough that the double layer ions cannot follow the field, and compare their phase behavior with Monte Carlo simulations of hard cubic particles, each containing a point dipole at their center, oriented along the field direction. We also explore whether the electric field can overcome the strong gravitational effects on self-assembly of this system of relatively heavy cubes in the experiments. In both simulations and experiments, we find a string fluid phase, a BCT crystal phase, and a hexagonally ordered columnar phase. By observing the behavior of the system in Monte Carlo simulations, we find both partial alignment of the particles in the string fluid and columnar crystal phases, and complete 3D alignment in the BCT phase.

Methods and model

Particle synthesis and suspensions

Cube-shaped particles of sodium magnesium fluoride (neighborite, $NaMgF_3$) are synthesized following the method by Sevonkaev *et al.*[46] The crystalline structure of neighborite is orthorhombic.[47] Sharp-edged cubic colloidal particles of 1.10 μm size are prepared as follows: 10 ml of 0.2 M aqueous magnesium chloride ($MgCl_2$) and 100 ml of 0.2 M aqueous sodium fluoride (NaF) solutions are mixed in a 500 ml laboratory flask. The flask is then immersed in a silicone oil bath maintained at 80 °C, and stirred at 100 rpm. The reaction is allowed to proceed, at constant temperature, for three hours. After the synthesis, the reaction mixture is washed 3–4 times with de-ionized water (18.2 MΩ cm, Millipore) to remove smaller particles and also unreacted species. Subsequently, the supernatant is removed and the particles in the sediment are redispersed in de-ionized water. Scanning and transmission electron micrographs of synthesized particles after cleaning are shown in Fig. 1. The average size and standard deviation were measured using iTEM imaging software (Olympus Soft Imaging Solutions). The polydispersity was calculated by dividing the standard deviation of the edge length σ of the cubes by the average edge length. For each sample, 80 to 100 particles were measured. The size and the polydispersity of the particles are $\sigma = 1.10$ μm and 8% respectively. The density and refractive index of the particles are 3.05 g cm^{-3} and 1.364 respectively.[46] The dielectric constant of the particles is 4.50.[47]

Our suspensions consist of positively charged $NaMgF_3$ cubic particles in water. Because our particles are positively charged, they tend to stick to the negatively charged glass walls of the sample cell. Before using the cell we coat its inside with a cationic polyelectrolyte (polyethyleneimine, PEI ($M_w = 750$ kg mol^{-1})). We flush a 0.5% by weight PEI aqueous solution through the cell. After filling the cell with the colloidal suspension, we seal it with UV-curing optical adhesive (Norland no. 68). Particle dynamics are followed by bright field microscopy using a charge coupled device (CCD) camera (UNIQ, UP-600). Although no salt is added, the conductivity is measured (390 μS cm^{-1}) for the dispersion of cubes (concentration 0.1%). This background concentration of ions could be due to dissolved CO_2 and/or slight dissolution of the cubes. We estimated the Debye screening length (66 nm) from the measured conductivity. We measured the conductivity with a CDM 230 conductivity meter (Radiometer analytical).

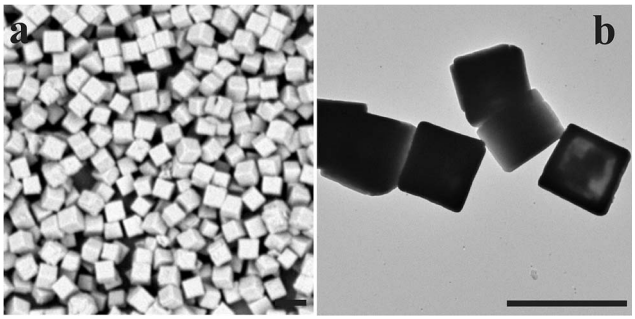

Fig. 1 Neighborite ($NaMgF_3$) sharp-edged colloidal cubes. (a) Scanning electron micrograph reveals that the particles are sharp-edged. (b) Transmission electron micrograph of the particles. The scale bar is 2 μm.

Electric field setup

We use two types of sample cells: rectangular capillaries (VitroCom, UK) and home made sandwich indium tin oxide (ITO) coated glass cells.[8] The rectangular sample cells consist of a 0.1 mm × 1.0 mm capillary with two 50 μm thick nickel-alloy wires (Goodfellow, UK) threaded along the side walls. Our sandwich ITO coated glass cell consists of two parallel no. 1 glass cover slips (130–160 μm thick, Menzel), which are completely coated with a conductive, semi-transparent layer of indium tin oxide (ITO, Diamond coatings limited, UK). They are kept apart by a pair of glass spacers, which are cut out of no. 1 or no. 0 (80–120 μm thick) slides and are placed at opposite sides of the sample space. Typically, the height of the sample space, enclosed by the cover slips, is 100–200 μm, with an area of ~1 cm^2. The conductive ITO layer is in direct contact with the suspension. The whole cell is constructed on top of a 1.0 mm thick microscopy slide, for extra support and easy mounting on the stage of the microscope. We glue everything together with no. 71 UV-curing optical adhesive (Norland). For the electrical contacts with the ITO electrodes we use silver paint (Jeol) and a thin thermocouple alloy wire (diameter 50 μm, Goodfellow), which is then wrapped around a standard electronic wire. We use a function generator (Agilent, Model 3312 OA) and a wide band voltage amplifier (Krohn-Hite, Model 7602M) to generate the electric fields. The field strength and the frequency are measured using an oscilloscope (Tektronix, Model TDS3052).

We use a high frequency (1 MHz) field to prevent polarization of the electric double layer around particles.

Simulations

In the Monte Carlo (MC) simulations, we model the colloidal cube-shaped particles as perfect hard cubes with edge length σ and one or more point dipoles inside each particle. The interactions thus consist of a dipolar interaction between the cubes and a hard-core repulsion that prevents particles from overlapping. In the case where each particle contains a single dipole, the dipolar interaction potential between two particles i and j is given by:

$$\beta u_{\mathrm{dip}}(r_{ij}, \theta_{ij}) = \frac{\gamma}{2}\left(\frac{\sigma}{r_{ij}}\right)^3 (1 - 3\cos^2\theta_{ij}), \quad (1)$$

where r_{ij} denotes the center-of-mass distance between the two particles and θ_{ij} the angle between the distance vector between the particles and the direction of the field. The strength of the dipole interaction is given by the prefactor γ: the interaction potential between two particles separated by a distance σ along and perpendicular to the field direction is $-\gamma k_{\mathrm{B}}T$ and $(\gamma/2)k_{\mathrm{B}}T$, respectively. The prefactor γ is proportional to the square of the strength of the applied external field, and can be estimated from the dielectric constants of the particles and solvent (see Appendix). The long-range interactions are handled using Ewald summations.[48,49] To detect overlaps between two cubes, we use a triangular tessellation scheme.[50]

In the simplest approximation, the dipole interactions are modeled by a single point dipole in the middle of each cube. In this model, rotations do not affect the dipolar pair interaction between two cubes, and rotational order can only emerge due to the hard-core interactions. However, recent theoretical calculations using the coupled dipole method show that although at large distances the interaction between two polarizable cubes behave as a simple dipole–dipole interaction, at short distances this approximation fails.[29] In particular, the single-dipole approximation significantly underestimates attractions, while overestimating repulsions. As shown in ref. 29, deviations reach 20–30% for touching particles, but rapidly decrease at larger distances. To investigate the repercussions of this on the orientation energy and the potential energy of two cubes, we studied cubes containing multiple dipoles arranged in a simple cubic lattice aligned with the orientation of the particle. Thus, every particle is divided into $n \times n \times n$ smaller cubes, and a point dipole is placed in the center of each smaller cube. Each point dipole interacts with all other dipoles *via* eqn (1), with the interaction strength γ lowered by a factor n^3 to ensure that the total dipole moment of the particle remains the same. Even with multiple point dipoles in each particle, the potential energy of a single particle is independent of its orientation. On the other hand, the particle pair interaction is now a function of both the relative position of the two particles and their individual orientations. While at high field strengths, this could affect the alignment of neighboring particles, this effect appears to be small (see Appendix) under conditions resembling the experimental system of this study. We therefore use the single-dipole approximation in the remainder of this work. However, we mention here that the dipolar interaction between cubes with multiple permanent dipole moments deviates from the more accurate field-induced dipolar interaction as calculated self-consistently using the coupled dipole method.[29]

An additional approximation made in the simulations is that the cubes are modeled as hard particles. Although our particles are positively charged, the Debye screening length in our system is small ($\approx$66 nm). Therefore, we believe that using a hard-core interaction potential in the simulations is a valid approximation. Broadly, we expect that adding a repulsive electrostatic interaction would have two main effects: the charge repulsions will (i) partly counteract the dipolar attractions that favor string formation and crystallization, and (ii) will increase the stability of low-density crystals, since the freezing transition will shift to a lower packing fraction as the effective diameter of the soft repulsive spheres will increase. Analogous to earlier studies on dipolar uncharged and charged spherical particles,[16] we therefore expect our simulations to underestimate the field strengths associated with all phase transitions, and to overestimate the coexistence densities associated with any fluid-crystal transition. Additionally, it cannot be excluded that sufficient charge repulsion could stabilize new crystal structures. However, we note that we have seen no signs of crystal structures in the experiments that were not observed in the simulations.

To investigate the phase behavior of the cubes, we performed Monte Carlo simulations in the *NPT* ensemble, *i.e.* at a fixed number of particles $N = 512$, pressure P and temperature T. The Monte Carlo moves used were single-particle translation and rotation moves, volume moves, and cluster translation moves.[48] In a single-particle translation move, a random particle was chosen and translated by a random displacement vector. The rotation move rotated a particle by a randomly chosen angle around the x, y, or z-axis (chosen at random). In the volume moves, we increased or decreased the simulation volume by a random amount, and then rescaled both the simulation box and all particle positions to match the new box volume. Finally, the cluster moves were identical to the single-particle translation moves, with the exception that all particles that were part of the same cluster as the chosen initial particle were translated as well. Here, two particles were considered to be part of the same cluster based on a cutoff distance. To maintain the detailed balance, any cluster move that changed the size of the translated cluster (by moving it too close to another particle) was rejected.[48] We note here that the addition of cluster moves significantly improved the equilibration in the low-density string-fluid phase, but did not improve the equilibration of crystalline phases. Therefore, we did not employ cluster moves in simulations at high pressure.

Simulations were performed in a series where the pressure was either increased or reduced slightly in each successive simulation, leading to compression or expansion of the system. During the compression runs, the simulations typically started from an initial configuration in the fluid phase, and the pressure was increased in small steps, up to pressures well beyond the expected bulk coexistence pressure. Expansion runs started from an initial configuration in one of the crystal phases that we

expect to be stable for the field strength γ used in the simulations. Phase transitions in the simulations were determined by examining the hysteresis in the density and crystalline order in simulation runs starting from different initial states. To quantify the crystalline order, we used both the orientational bond-order parameter q_4 (ref. 51) to detect cubic symmetry (such as present in the body-centered tetragonal and simple cubic crystal structures), and the two-dimensional ϕ_6 order parameter to determine the hexagonal ordering of the strings in the hexagonal columnar phase. We then estimated phase transition lines by locating jumps in the density and crystallinity as a function of the pressure and by visually inspecting snapshots of simulations performed in these regions. In the regimes where the hysteresis region is very small (*i.e.* where the phase transition occurs at the same point regardless of the initial state of the simulation), this method gives an accurate estimate of the transition point. This is true for all crystal–crystal coexistences, and thus we expect the errors in the coexistence lines to be small ($\lesssim$2% in the packing fraction). However, the transition between the string fluid and the hexagonal columnar phase shows a large degree of hysteresis. As a result, the determined fluid-hexagonal coexistence densities are less accurate, with estimated errors $\lesssim$5% in the packing fraction.

In the fluid phase, the cubes self-assemble into strings as the dipolar interactions favor the head-to-tail alignment of the point dipoles. At high field strengths, these strings span the simulation box, and it is likely that the phase behavior of the system in this regime is affected by finite size effects. To investigate this, the simulations for high field strengths ($\gamma \geq 12.5$) and low pressures ($P\sigma^3/k_BT < 1$) were also performed in a system of $N = 1024$ particles. We observed no significant shift in the phase boundaries.

To determine the transition from a simple cubic (SC) to a body-centered tetragonal (BCT) crystal structure, we performed simulations at constant pressure for a range of field strength γ, starting from either of the two phases. We identify the switch between the two crystal phases by monitoring the potential energy and *via* visual inspection. Since the system can easily switch between the two structures, no clear hysteresis was visible in these simulations, and determining the approximate phase boundaries was straightforward, resulting in estimated errors $\lesssim$5% in the field strength γ.

Results

Phase diagram from simulations

Fig. 2 shows the phase diagram for colloidal hard cubes in an electric field, as a function of the field strength γ and the packing fraction η, determined using *NPT* Monte Carlo simulations. The phase behavior bears close resemblance to that of dipolar hard spheres,[16] with the main difference being the added hexagonal string phase. This phase consists of strings of cubes along the field direction, with the strings arranged on a hexagonal lattice, but no clear correlation between the positions of particles within different strings. Additionally, in this phase the cubes show no orientational alignment with respect to rotation around the field axis. For this structure, the lowest

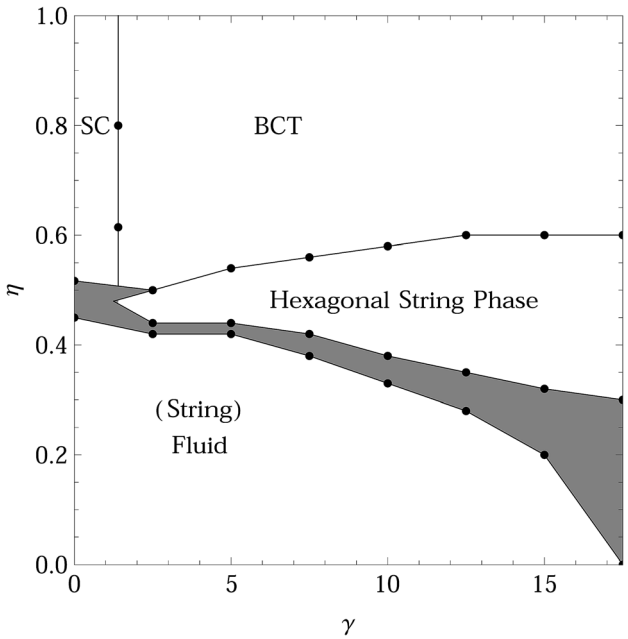

Fig. 2 Phase diagram for colloidal hard cubes in an external electric or magnetic field, as a function of the field strength γ and the packing fraction η. The black points indicate where phase boundaries were determined based on the phases found in MC simulations at constant pressure. The labels SC and BCT denote a simple cubic and a body-centered tetragonal phase, respectively, while the hexagonal phase consists of strings of particles arranged on a hexagonal lattice.

energy state would likely have three of the six neighbors of each string shifted up by a third of the inter-particle distance in a string, and the other three shifted down by the same amount, but this order is not clearly visible in the simulations. In fact, the particles in the simulations are mobile along the string direction, although it is likely that such movement would become progressively more difficult for larger system sizes. For a typical snapshot, see Fig. 3a. The hexagonal arrangement maximizes the distance between strings, allowing for larger orientational entropy at the cost of a higher potential energy. The hexagonal phase coexists with a fluid phase at lower volume fraction, which lacks (semi) long-range order in the plane perpendicular to the E-field and in addition has long-time self diffusion of the strings in this plane. The fluid-hexagonal coexistence region becomes broader upon increasing the field strength. In the limit of high field strengths, the hexagonal columnar phase is expected to vanish eventually (not shown in Fig. 2) based on energetic arguments: the BCT phase has a lower potential energy, and will only coexist with a dilute gas at sufficiently high interaction strengths. However, due to the sharp decrease in particle mobility in our simulations for interaction strengths higher than $\gamma \simeq 15$, we were unable to determine at which field strength the hexagonal phase will vanish.

The other difference between the phase diagrams for cubes (Fig. 2) and spheres (ref. 16) in external fields is the crystal structure present at low field strengths. The FCC crystal structure that is stable in this region for dipolar hard spheres is

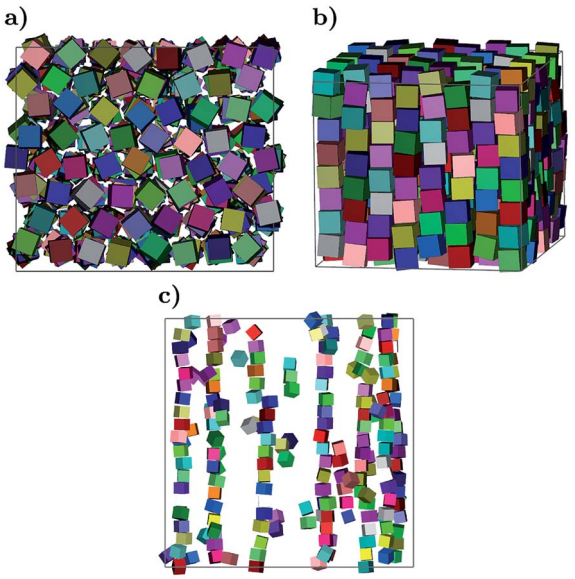

Fig. 3 (a) Snapshot of the hexagonal phase, at $\gamma = 15$ and $\beta P\sigma^3 = 1.5$ ($\eta = 0.46$). The field direction is perpendicular to the plane of view. (b) Snapshot of the BCT phase, at $\gamma = 15$ and pressure $\beta P\sigma^3 = 4$ ($\eta = 0.64$). The external field points along the vertical direction. (c) Snapshot of a dilute string fluid phase, at $\gamma = 14$ and $\eta = 0.02$. The field direction is vertical.

replaced by a simple cubic (SC) crystal in the case of cube-shaped particles. This structure is also stable for hard cubes without external fields.[39] Although the structure remains largely cubic, the simple cubic phase is slightly distorted as the field strength is increased: the lattice is compressed along the field direction due to the dipolar interactions, depending on the strength of the interactions and the packing fraction. The maximum packing fraction of the SC phase of sharp cubes is $\eta = 1$. At this packing fraction, all cubes are aligned along the same three axes, but a limited amount of freedom remains for the positions of the particles. However, the lowest energy state at $\eta = 1$ is a body-centered tetragonal (BCT) structure, and we thus observe a transition from a SC to a BCT phase upon increasing the electric field strength. The BCT structure consists of strings of cubes on a square lattice, with all the particles aligned. Each string is shifted along the field direction with respect to its four neighboring strings by a distance equal to half of the lattice spacing. A typical snapshot of this structure is shown in Fig. 3b. We note that the stability of this phase is likely enhanced slightly by the single-dipole approximation used to model the dipolar interactions: spreading out the dipole moment over the cube would result in a weaker preference for configurations where neighboring strings are shifted with respect to each other.

As in the case of hard spheres in an external electric field, a string fluid appears for low field strengths and low packing fractions. Neighboring cubes in a string are aligned such that the touching faces of the two cubes are approximately parallel, as this allows the point dipoles to approach each other more closely (see Fig. 3c for a typical snapshot). Because aligning the cubes along this direction carries an entropic cost, the strings formed by cubes are typically slightly shorter than those formed by spheres (at the same value of γ). Since the cubes only contain a single point dipole, rotations along the field axis do not influence the potential energy of the system. As a result, the cubes do not align all faces within a single string: there is only alignment along the field. In the case of multiple point dipoles in each cube, we also find that there is no alignment of the cubes perpendicular to the field for field strength $\gamma < 30$ (see Appendix). Hard-core interactions with neighboring strings or a wall could cause the particles to align in all three directions. This indeed occurs in the BCT phase at sufficiently high packing fractions.

Experimental results

Our experimental system consists of positively charged cube-shaped sodium magnesium fluoride (neighborite) particles in water (Fig. 4a). The particles sediment quickly to the bottom due to their high density (3.05 g cm^{-3}), thereby increasing the volume fraction. On the single-particle level, the gravitational length l_g, which characterizes at what height differences gravity will start to play an important role in the equilibrium phase behavior,[18,52] is approximately $l_g = 0.15\ \mu\text{m} \simeq 0.14\sigma$, for this reason we investigate both configurations with the electric field parallel and perpendicular to the direction of gravity. However, induced dipolar attractions between the particles are typically strong enough to overcome gravitational effects when a sufficiently strong field is applied parallel to the direction of gravity.[53] Unfortunately, it is not possible to follow the behavior of individual particles as a function of time in concentrated systems, as neither the particles nor the solvent is labeled with a fluorescent dye, and the refractive indices of the solvent and particles were not well matched, thus making the use of confocal microscopy practically impossible. Therefore, we restrict our studies to microscopic imaging close to the cell boundary, essentially in two dimensions and to some extent only qualitatively with respect to exact orientations of the cubes, although particles that are not in focus also contribute to the image. By using two types of electric cells we are able to observe the structures in two mutually perpendicular planes. However, for the configuration where gravity is perpendicular to the applied electric field and for both geometries at low field strengths and volume fractions, the particles sediment relatively quick to the bottom of the electric cells. We first investigate the behavior of the particles in the dilute regime. Upon application of an electric field the cubes acquire an induced dipole moment due to the difference in dielectric constant between the particles and the solvent. As expected, this causes the particles to self-assemble into string-like clusters (see Fig. 4) parallel to the field directions. However, the potential energy of a single cube in an electric field is independent of its orientation as the polarization tensor is isotropic.[27] As a consequence, we expect the colloidal cubes to rotate freely in the electric field. In our experiments, we indeed see no preferential orientation of single particles. Non-clustered particles appear to rotate freely, as demonstrated by the cube indicated by the arrows in Fig. 4b–f. On the other hand, for clustered particles, the hard-core

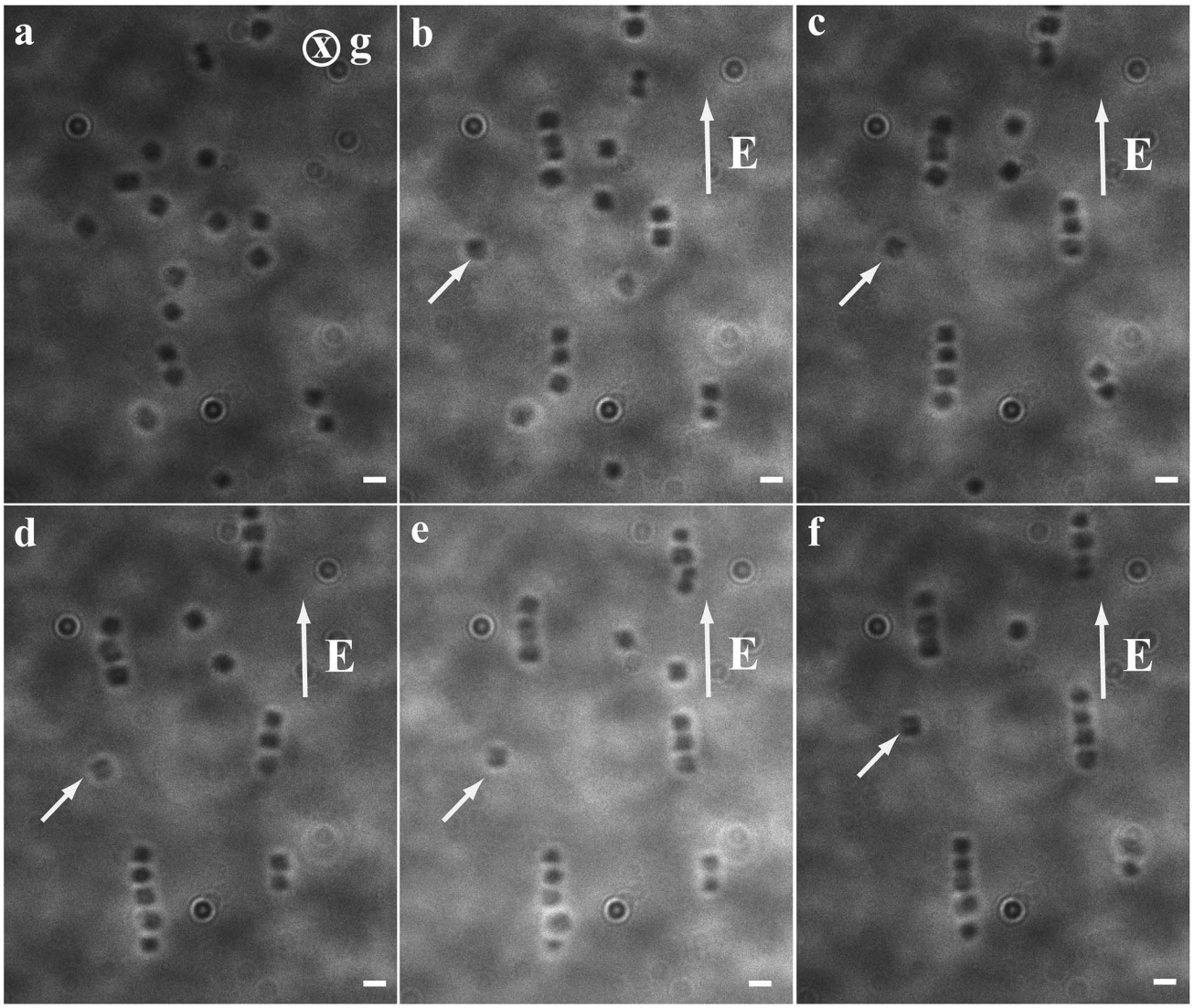

Fig. 4 Time-lapse optical microscopy images of sharp-edged cubic particles in an electric field. Gravity is directed perpendicular to the plane of view, and the external field points in the vertical direction. (a) Isotropically dispersed particles at zero field strength. (b–f) At a low field strength ($E_{rms} = 0.02$ V μm^{-1}, at a frequency of 1 MHz), particles preferentially align in a head-to-tail fashion along the field direction, while a single cube does not show any preferential orientation. The arrow indicates the different orientations of the single cube. The time lapse between the frames is 2 s. The scale bar is 2 μm.

interactions between the cubes lead to alignment (see Fig. 4b–f), where the cubes are oriented with two planes perpendicular to the field direction, such that the centers of neighboring particles can approach each other as closely as possible. As far as we can tell, the particles in a string still rotate freely around the field direction, in agreement with our simulations.

At a higher volume fraction $\eta \approx 0.60$, long strings of particles form in the suspension (Fig. 5b), within seconds after applying a field strength of $E_{rms} = 0.03$ V μm^{-1}. Moreover, the particles are oriented along the direction of the applied electric field. Similar to the behavior of spheres in electric fields, we observe a preferential offset of half a particle diameter between neighboring strings, such that the particles locally form a distorted hexagonal pattern. This minimizes the dipolar repulsion between particles in the plane perpendicular to the electric field. At this volume fraction, neighboring cubes in a string are aligned such that the adjacent faces of two cubes are approximately parallel, due to the hard-core interactions. As a result, all faces of the cubes are aligned within a single string as shown in the inset of Fig. 5b. Hard-core interactions with neighboring strings and the bottom flat wall could cause the particles to align in all three directions. We also observe (see Fig. 5b) that the particles are orientationally ordered along the direction of the applied field. However, we are not able to observe the rotation of the particles around the field axis. We believe that the strings possess orientational order in that direction due to sedimentation of the strings on a flat wall. Additionally, the particles possess positional order within a string along the applied field direction while no long-range positional correlations exist between

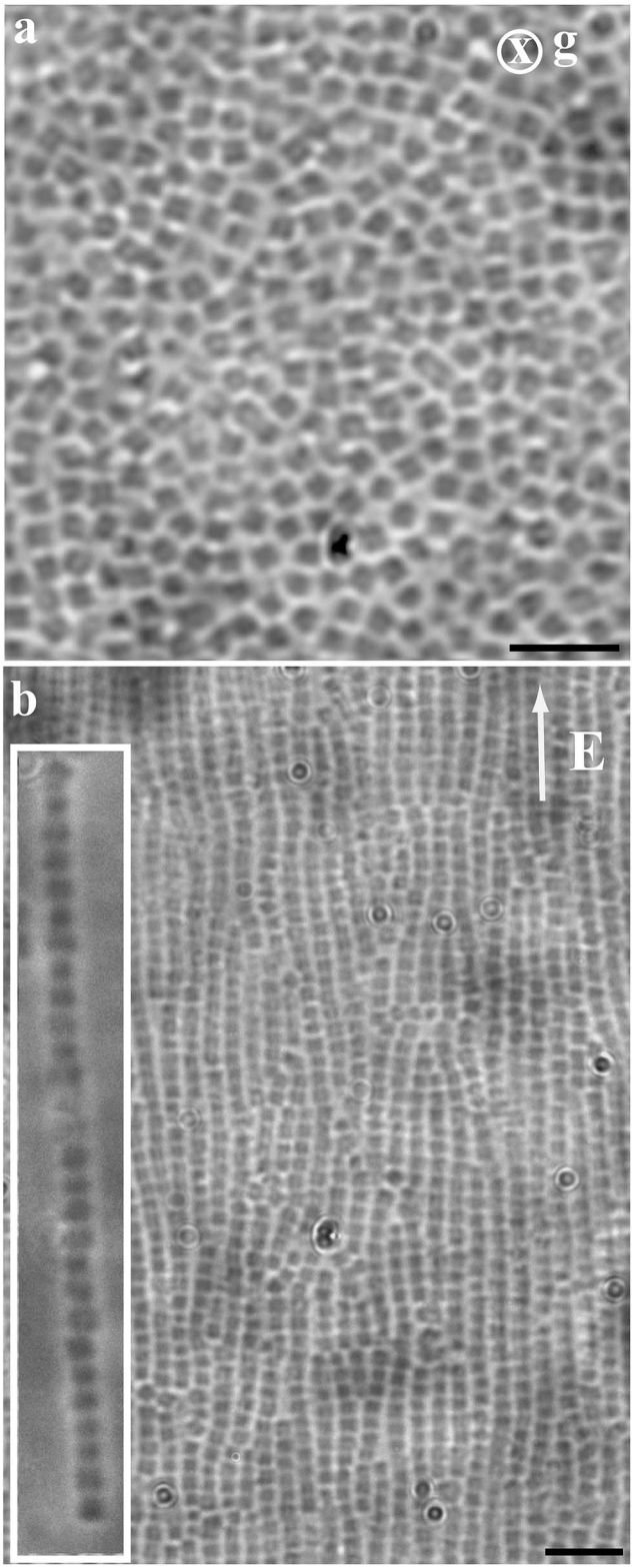

Fig. 5 Optical micrographs of cube-shaped neighborite ($NaMgF_3$) particles in an external electric field. (a) Isotropically dispersed particles at zero field strength. (b) Particles were aligned along the field direction at field strength ($E_{rms} = 0.04$ V μm^{-1}). (Left inset) A magnified view of a single string. We note that images were recorded close to the glass wall at the bottom of the capillary. The scale bar is 5 μm.

neighboring strings. Therefore, this phase corresponds to a dense string fluid phase.

From the difference in dielectric constant between the particles and solvent and the applied field strength, we estimate that the prefactor in this case corresponds to $\gamma/k_BT \approx 63$ (see Appendix). At these high field strengths, our simulations only predict a dilute gas phase in coexistence with a crystal phase, and no dense string fluids. Possible reasons for the observed discrepancies between the experimental γ values and the simulations are the polydispersity of the experimental system, the porous nature of the particles (which would result in an effective dielectric constant closer to that of the solvent), and the net positive charge of the particles in the experiments, which would partially counteract the dipolar attractions. Additionally, in our simulations we approximated the inter-particle dipolar interactions using a simple point-dipole approximation which neglects the field generated by other particles.

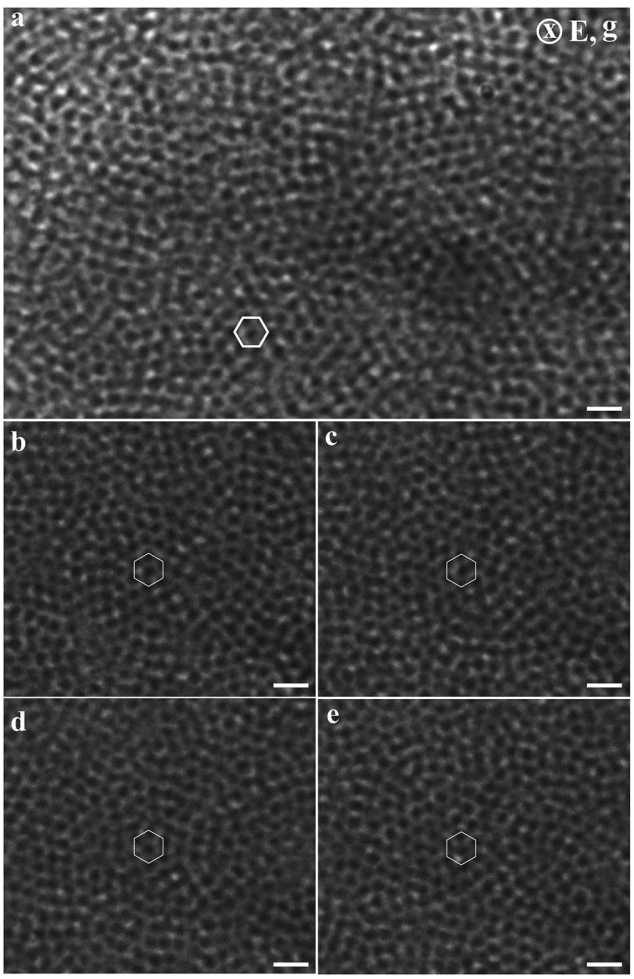

Fig. 6 Optical micrographs of hexagonally ordered strings of rotationally disordered cubes at $\eta = 0.60$. (a) 2D snapshot reveals the hexagonal arrangement of strings at intermediate field strengths (E_{rms} = 0.06–0.10 V μm^{-1}). The skewed white hexagon indicates the arrangement of the cubes. (b–e) Series of *xy* images showing the change in orientation of the individual cubes in an electric field. The time lapse between the frames is 2 s. The scale bar is 3 μm.

To observe the order in a plane perpendicular to the field, we used a sandwich ITO coated cell. At high field strengths (E_{rms} = 0.06–0.10 V μm^{-1}) and a particle concentration of $\eta \approx 0.60$, the particles formed a hexagonal arrangement of strings which are rotationally disordered around the applied field direction as shown in Fig. 6. Although we were unable to follow rotations of the particles on a single particle level, we could see that the particles were rotationally disordered as seen in Fig. 6b–e. This is consistent with the hexagonal columnar phase observed in the simulations. Moreover, multiple hexagonal domains with different orientations were observed. We observed this structural change within 25–30 min. We followed the structure over a period of 2 days, but did not observe any long-range hexagonal positional order in the system. In addition, we did not see any structural changes at even higher field strengths ($E_{rms} \geq 0.20$ V μm^{-1}). We suspect that the system might be out of equilibrium, due to the strong effects of the dipolar interactions and gravity. When we switched off the field, the suspension returned to a fluid state, indicating that this structure was indeed the result of induced dipolar interactions.

Our simulations show that the body-centered tetragonal phase is stable at high field strengths and densities. To test these predictions, we used a dispersion with an initial volume fraction of $\eta \approx 0.45$. We let the sample sediment for about 40–45 min to obtain a volume fraction of $\eta \approx 0.85$ close to the bottom. Subsequently, the dispersion was exposed to high field strengths ($E_{rms} \geq 0.20$ V μm^{-1}). At this high field strength, the strings spanned the gap between the two electrodes, offsetting gravity because of the (much) stronger dipolar interactions. After 1–1.5 h, the strings slowly transformed from a fluid to a square-like arrangement due to strong induced dipolar interactions. Unfortunately, our particles are non-fluorescent therefore we could not follow the particles in the *z*-direction. As a result, it is hard to determine whether a string is shifted along the field direction by a distance equal to half of the lattice spacing with respect to its neighbors, as we would expect from the simulation results. Nonetheless, optical micrographs (Fig. 7) clearly show small domains with the square arrangement of particles in planes perpendicular to the applied field, consistent with a BCT structure. These results also show that in this configuration, similar to spheres, the effects of gravity can be mostly offset as they can be made small compared to the dipolar energies involved.

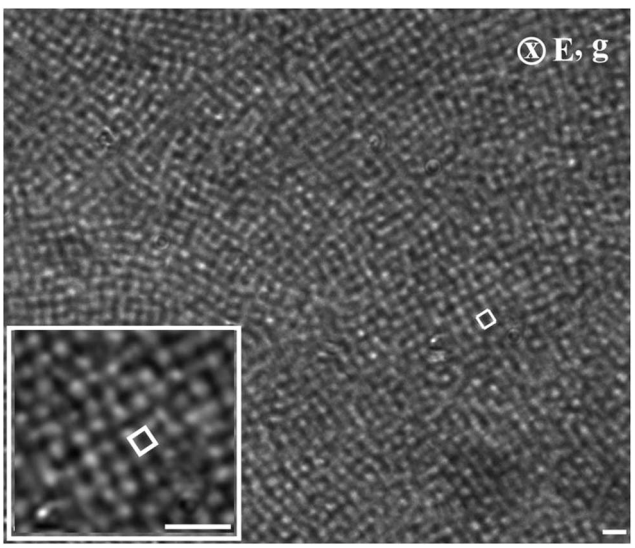

Fig. 7 Optical micrograph of the square arrangement of strings of particles, highlighted by the white square. The image (*xy*) clearly shows indications of the characteristic BCT stacking: square arrangement of cubes perpendicular to the applied field (E_{rms} = 0.13 V μm^{-1}). The inset shows a magnified view of the square arrangement. The scale bar is 4 μm.

Conclusions

In summary, we studied the phase behavior of hard colloidal cubes in an external electric field. Experiments using optical microscopy in suspensions of neighborite cubes show the formation of strings at low densities, and hexagonal and square domains at high densities, depending on the external field strength. The phase behavior can be understood using a simple model consisting of hard cubes containing a single point dipole. The phase diagram of this model contains body-centered tetragonal and simple cubic crystal phases, a hexagonal columnar phase, and a string fluid phase, in good qualitative agreement with our experimental observations.

Interestingly, while the electric field does not induce alignment in individual cubes, the application of the field nonetheless allows control over the orientation of the particles: the formation of strings causes the particles to prefer orientations where one of the faces is perpendicular to the field direction, similar to the para-nematic phase formed by rod-shaped particles in external fields.[23,54] At low to intermediate densities, in the string fluid and hexagonal columnar phases, this leaves the particles free to rotate only around the field axis. At higher densities, or in the presence of a hard wall placed parallel to the field, the additional excluded volume effects can instead induce full orientational order in the cubes. In short, external electric fields form a useful tool for controlling the orientation and structure of cube-shaped colloidal particles including the ability to reduce the effects of gravity on self-assembly even for relatively heavy micron-sized cubes. This is important as until now almost all experimental research on cube shaped particles focused on 2D or very thin 3D samples. As the effects of the cubic particle shape strongly influence defects in the solids of hard cubes[39] this finding makes it worthwhile to try to develop a fluorescent version of this model system for more quantitative 3D results in the future.

Appendix: point-dipole approximation

Calculation of the prefactor γ

Comparing experimental results to simulations requires a mapping between the experimental electric field strength and the prefactor γ in eqn (1). In the approximation of the single point-dipole model used here, a natural method to do this is to estimate the total effective dipole moment the particle obtains in the external field. For a particle with volume σ^3 and dielectric

constant ε_p suspended in a solvent with dielectric constant ε_s and an applied external field $\mathbf{E}_0$, the dipole moment $\mathbf{p}$ can be estimated using the Clausius–Mossotti relationship:[55]

$$\mathbf{p} = 3\varepsilon_s\varepsilon_0\left(\frac{\varepsilon_p - \varepsilon_s}{\varepsilon_p + 2\varepsilon_s}\right)\sigma^3\mathbf{E}_0, \quad (2)$$

with ε_0 is the vacuum permittivity. The interaction energy between two point dipoles $\mathbf{p}$ separated by a distance $\sigma\hat{\mathbf{p}}$ is given by:

$$U_{dip} = \frac{-1}{4\pi\varepsilon_s\varepsilon_0}\frac{2p^2}{\sigma^3}. \quad (3)$$

Using eqn (1), we see that this should equal $-\gamma k_B T$. Thus, for the prefactor γ, we obtain:

$$\gamma = \frac{9\sigma^3}{2\pi}\frac{\varepsilon_s\varepsilon_0}{k_B T}\left(\frac{\varepsilon_p - \varepsilon_s}{\varepsilon_p + 2\varepsilon_s}\right)^2 {E_0}^2. \quad (4)$$

For the system under consideration here, using the experimental parameters, $\gamma \approx 7 \times 10^4 {E_{rms}}^2$ ($\mu m^2\ V^{-2}$).

We note that strictly speaking, the Clausius–Mossotti relationship only applies to spherical particles: in general one should take into account the fact that the electric field inside the particle is not necessarily parallel to the external field. For a discussion of this, and of the limitations of the single point-dipole approach for cube-shaped particles, see ref. 29.

Estimation of aligning forces in the string fluid

Simulations of a string fluid of cubic particles show that the top and bottom faces of neighboring particles in the directions perpendicular to the field are aligned in order to minimize the distance between them, whereas the particles are free to rotate around the field axis. This can be understood from the way the interactions are modeled: since the pair potential in eqn (1) only depends on the positions of the centers of the particles, there is no way for it to align the particles orientationally. It is possible that in a more realistic model aligning forces may exist as a result of the way cube-shape particles are polarized in the external field.

As a simple estimate of how strong such forces would be, we use a slightly more complex model, approximating the polarization of the cube with multiple dipoles evenly spread through the particle. While this still neglects any variations in the strength and orientation of the local polarization in the particle, this should give a first-order approximation of the effect of the particle shape on the dipolar forces. Thus, we divide each cube into $n \times n \times n$ smaller cubes (on a simple cubic lattice), and place a weaker dipole in the middle of each smaller cube, keeping the total dipole moment of a particle fixed. Calculating the potential energy for different configurations of two particles in a string-like configuration shows that the potential energy difference between different orientations is small compared to the total interaction energy. For eight dipoles in each cube, the difference between the perfect alignment and the maximum misalignment (45°) is only around $0.04\gamma k_B T$. While this difference will induce alignment at very high field strengths, the effect will be small below $\gamma \approx 25$, corresponding to a field strength of 0.02 V μm^{-1} for our experimental setup. Moreover, for particles containing more than 8 point dipoles, the effect of rotations on the potential energy slowly decreases with the number of dipoles (see Fig. 8). The energy difference appears to level off around $0.01\gamma k_B T$, which would indicate that a prefactor $\gamma \gtrsim 100$ would be needed to significantly align particles with the electric field, corresponding to $E_{rms} = 0.04$ V μm^{-1} in our case. As the string fluid is no longer stable at this field strength, it would be impossible to notice this effect under equilibrium circumstances. We also performed simulations of cubes containing eight point dipoles, and studied the alignment of particles in a string as a function of the field strength. Neighboring particles were seen to visibly align in strings at field strengths higher than $\gamma \approx 30$, but for lower field strengths, no clear correlations in the orientations of neighboring particles were visible. Since the energy calculations show that the alignment effect decreases in strength on increasing the number of point dipoles per particle, we conclude that for a field strength lower than $\gamma = 30$ using multiple point dipoles per particle is not likely to significantly influence the alignment of cubes in the string fluid phase or the hexagonal columnar phase.

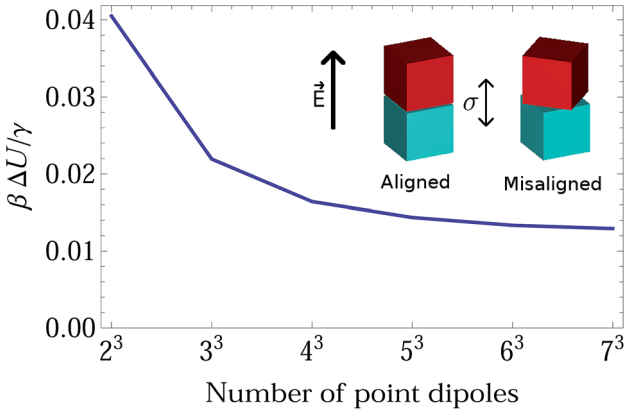

Fig. 8 Energy difference ΔU between the most favorable (aligned) and least favorable (misaligned) orientations of two particles at distance σ along the z-axis, for different numbers of point dipoles per particle. The inset depicts the aligned (left) and misaligned (right) orientations.

Acknowledgements

We acknowledge the support from an NWO-VICI grant, and this work is part of the research programme of the Foundation for Fundamental Research on Matter (FOM), which is part of the Netherlands Organisation for Scientific Research (NWO). Additionally, this study is part of the FOM/DFG collaborative Transregio Network 6 on Colloids in External Fields.

References

1 S. C. Glotzer and M. J. Solomon, *Nat. Mater.*, 2007, **6**, 557.
2 A. Stein, F. Li and N. R. Denny, *Chem. Mater.*, 2008, **20**, 649.

3 S. M. Yang, S. H. Kim, J. M. Lim and G. R. Yi, *J. Mater. Chem.*, 2008, **18**, 2177.
4 M. Grzelczak, J. Vermant, E. M. Furst and L. M. Liz-Marzan, *ACS Nano*, 2010, **4**, 3591.
5 E. Duguet, A. Désert, A. Perrozab and S. Ravaine, *Chem. Soc. Rev.*, 2011, **40**, 941.
6 K. D. Hermanson, *et al.*, *Science*, 2001, **294**, 1082.
7 H. R. Vutukuri, *et al.*, *Adv. Mater.*, 2012, **24**, 412.
8 H. R. Vutukuri, *et al.*, *Angew. Chem.*, 2012, **124**, 11411.
9 B. Peng, H. R. Vutukuri, A. van Blaaderen and A. Imhof, *J. Mater. Chem.*, 2012, **22**, 21893.
10 M. E. Leunissen, H. R. Vutukuri and A. van Blaaderen, *Adv. Mater.*, 2009, **21**, 3116.
11 J. E. Martin, R. A. Anderson and R. L. Williamson, *J. Chem. Phys.*, 2003, **118**, 1557.
12 J. E. Martin, R. A. Anderson and C. P. Tigges, *J. Chem. Phys.*, 1998, **108**, 7887.
13 A. Yethiraj and A. van Blaaderen, *Nature*, 2003, **421**, 513.
14 A. Yethiraj, *Soft Matter*, 2007, **3**, 1099.
15 A. van Blaaderen, *et al.*, *Eur. Phys. J. Spec. Top.*, 2013, **222**, 2895.
16 A.-P. Hynninen and M. Dijkstra, *Phys. Rev. Lett.*, 2005, **94**, 138303.
17 A.-P. Hynninen and M. Dijkstra, *Phys. Rev. E: Stat., Nonlinear, Soft Matter Phys.*, 2005, **72**, 051402.
18 A. Yethiraj, A. Wouterse, B. Groh and A. van Blaaderen, *Phys. Rev. Lett.*, 2004, **92**, 058301.
19 G. M. Range and S. H. L. Klapp, *J. Chem. Phys.*, 2005, **122**, 224902.
20 F. Smallenburg, *et al.*, *J. Phys.: Condens. Matter*, 2012, **24**, 464113.
21 N. Elsner, C. P. Royall, B. Vincent and D. R. E. Snoswell, *J. Chem. Phys.*, 2009, **130**, 154901.
22 F. Smallenburg and M. Dijkstra, *J. Chem. Phys.*, 2010, **132**, 204508.
23 K. Chaudhary, *et al.*, *Soft Matter*, 2014, **10**, 1320.
24 A. Kuijk, *et al.*, *Soft Matter*, 2014, **10**, 6249.
25 A. F. Demirors, *et al.*, *Langmuir*, 2010, **26**, 14466.
26 B. Liu, *et al.*, *Nat. Commun.*, 2014, **5**, 3092.
27 B. W. Kwaadgras, M. Verdult, M. Dijkstra and R. van Roij, *J. Chem. Phys.*, 2011, **135**, 134105.
28 B. W. Kwaadgras, M. Dijkstra and R. van Roij, *J. Chem. Phys.*, 2012, **136**, 131102.
29 B. W. Kwaadgras, R. van Roij and M. Dijkstra, *J. Chem. Phys.*, 2014, **140**, 154901.
30 T. Sugimoto and K. Sakata, *J. Colloid Interface Sci.*, 1992, **152**, 587.
31 L. Rossi, *et al.*, *Soft Matter*, 2011, **7**, 4139.
32 C. J. Murphy, *et al.*, *J. Phys. Chem. B*, 2005, **109**, 13857.
33 H.-J. Yang, S.-Y. He, H.-L. Chen and H.-Y. Tuan, *Chem. Mater.*, 2014, **26**, 1785.
34 Z. Pu, *et al.*, *Nanotechnology*, 2006, **17**, 799.
35 L. Gou and C. J. Murphy, *Nano Lett.*, 2003, **3**, 231.
36 S. H. Im, Y. T. Lee, B. Wiley and Y. Xia, *Angew. Chem.*, 2005, **117**, 2192.
37 J. Ren and R. D. Tilley, *J. Am. Chem. Soc.*, 2007, **129**, 3287.
38 J.-M. Meijer, *et al.*, *Soft Matter*, 2013, **9**, 10729.
39 F. Smallenburg, L. Filion, M. Marechal and M. Dijkstra, *Proc. Natl. Acad. Sci. U. S. A.*, 2012, **109**, 17886.
40 U. Agarwal and F. A. Escobedo, *Nat. Mater.*, 2011, **10**, 230.
41 A. P. Gantapara, J. de Graaf, R. van Roij and M. Dijkstra, *Phys. Rev. Lett.*, 2013, **111**, 015501.
42 B. S. John, C. Juhlin and F. A. Escobedo, *J. Chem. Phys.*, 2008, **128**, 044909.
43 R. D. Batten, F. H. Stillinger and S. Torquato, *Phys. Rev. E: Stat., Nonlinear, Soft Matter Phys.*, 2010, **81**, 061105.
44 R. Ni, *et al.*, *Soft Matter*, 2012, **8**, 8826.
45 X. Zhang, Z. Zhang and S. C. Glotzer, *J. Phys. Chem. C*, 2007, **111**, 4132.
46 I. Sevonkaev, D. V. Goia and E. Matijevic, *J. Colloid Interface Sci.*, 2007, **317**, 130.
47 M. W. A. Bright and M. H. Lewis, *Am. Mineral.*, 1971, **56**, 1519.
48 D. Frenkel and B. Smit, *Understanding Molecular Simulations: From Algorithms to Applications*, Academic Press, San Diego, 2002.
49 P. P. Ewald, *Ann. Phys.*, 1921, **369**, 253.
50 J. de Graaf, R. van Roij and M. Dijkstra, *Phys. Rev. Lett.*, 2011, **107**, 155501.
51 P. R. ten Wolde, M. J. Ruiz-Montero and D. Frenkel, *J. Chem. Phys.*, 1996, **104**, 9932.
52 D. El Masri, *et al.*, *Soft Matter*, 2012, **8**, 6979.
53 U. Dassanayake, S. Fraden and A. van Blaaderen, *J. Chem. Phys.*, 2000, **112**, 3851.
54 M. Rotunno, T. Bellini, Y. Lansac and M. A. Glaser, *J. Chem. Phys.*, 2004, **121**, 5541.
55 M. Parthasarathy and D. J. Klingenberg, *Mater. Sci. Eng., R*, 1996, **17**, 57.